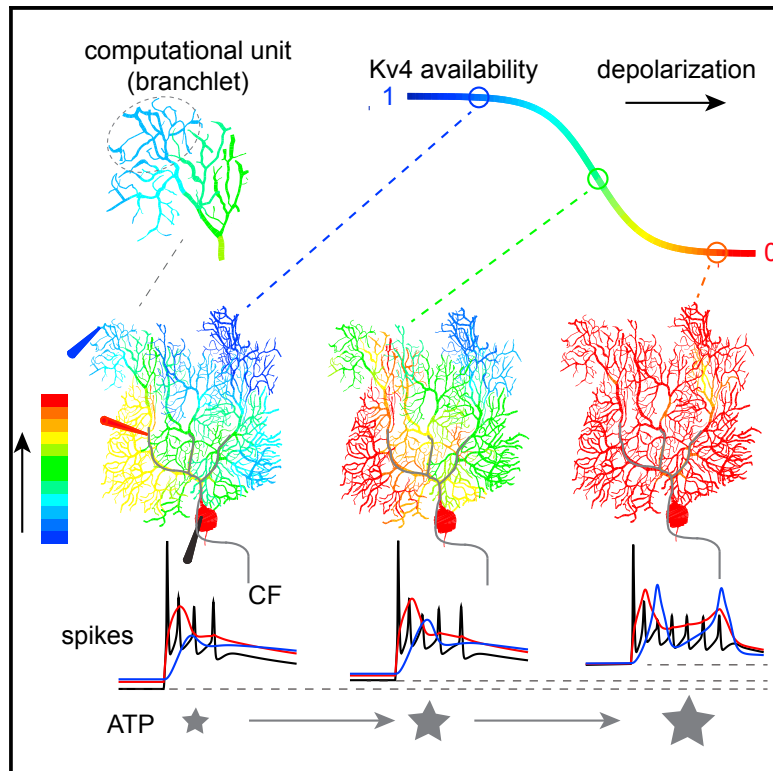


Voltage- and Branch-Specific Climbing Fiber Responses in Purkinje Cells

Graphical Abstract



Authors

Yunliang Zang, Stéphane Dieudonné,
Erik De Schutter

Correspondence

erik@oist.jp

In Brief

Zang et al. find that the availability of K^+ currents regulates Ca^{2+} influx and corresponding energy consumption during climbing fiber input in Purkinje cell dendrites. They systematically explore the mechanisms underlying variable somatic complex spikes and identify branchlet-specific computation in dendrites.

Highlights

- Voltage gates climbing fiber responses in Purkinje dendrites by activating K currents
- Energy consumption for complex spikes is voltage dependent
- Somatic complex spike duration does not predict climbing fiber bursting
- Climbing fiber responses in Purkinje cell dendrites are branchlet specific



Voltage- and Branch-Specific Climbing Fiber Responses in Purkinje Cells

Yunliang Zang,¹ Stéphane Dieudonné,² and Erik De Schutter^{1,3,*}

¹Computational Neuroscience Unit, Okinawa Institute of Science and Technology Graduate University, Okinawa 904-0495, Japan

²IBENS, Département de Biologie, Ecole Normale Supérieure, CNRS, INSERM, PSL Research University, 75005 Paris, France

³Lead Contact

*Correspondence: erik@oist.jp

<https://doi.org/10.1016/j.celrep.2018.07.011>

SUMMARY

Climbing fibers (CFs) provide instructive signals driving cerebellar learning, but mechanisms causing the variable CF responses in Purkinje cells (PCs) are not fully understood. Using a new experimentally validated PC model, we unveil the ionic mechanisms underlying CF-evoked distinct spike waveforms on different parts of the PC. We demonstrate that voltage can gate both the amplitude and the spatial range of CF-evoked Ca^{2+} influx by the availability of K^+ currents. This makes the energy consumed during a complex spike (CS) also voltage dependent. PC dendrites exhibit inhomogeneous excitability with individual branches as computational units for CF input. The variability of somatic CSs can be explained by voltage state, CF activation phase, and instantaneous CF firing rate. Concurrent clustered synaptic inputs affect CSs by modulating dendritic responses in a spatially precise way. The voltage- and branch-specific CF responses can increase dendritic computational capacity and enable PCs to actively integrate CF signals.

INTRODUCTION

According to the Marr-Albus-Ito theory (Albus, 1971; Ito, 1972; Marr, 1969), climbing fiber (CF) inputs to Purkinje cells (PCs) carry movement error information and evoke cerebellar learning by depressing the strength of parallel fiber (PF) synaptic input. Recently, processing of CF-carried error information by PCs has become a focus of cerebellar research (Najafi et al., 2014; Yang and Lisberger, 2014), with increased attention to modifiable dendritic responses (Davie et al., 2008; Kitamura and Häusser, 2011; Najafi et al., 2014; Rokni et al., 2009). Unfortunately, the biophysical mechanisms underlying the voltage-related dendritic response amplitude are still unresolved. CF provides powerful synaptic input onto proximal dendrites, but Ca^{2+} influx in distal dendrites is found to be unreliable (Ohtsuki et al., 2012; Otsu et al., 2014; Zagha et al., 2010). The pattern of dendritic spike initiation and propagation is important because the spatial range of Ca^{2+} influx controls the dendritic sites undergoing synaptic plasticity and even

the direction of cerebellar learning. Moreover, whether individual branches of PC dendritic trees are homogeneously excitable has never been investigated due to technical limitations. The effect of clustered PF synaptic input (Wilms and Häusser, 2015) on CF-evoked dendritic responses is also unknown. The answers to these questions will determine whether the computational unit of CF responses is the entire dendritic tree or individual branches.

Somatic complex spikes (CSs) were assumed to be a result of synaptic input current and somatic ionic currents (Schmolesky et al., 2002). Observations that dendritic spike variation plays a minimal role in evoking an extra somatic spikelet seemed to confirm this assumption (Davie et al., 2008); however, contrary observations exist (Ohtsuki et al., 2012; Otsu et al., 2014). Somatic CSs are quite variable (Burroughs et al., 2017; Warnaar et al., 2015) and their durations have been linked with the degree of trial-over-trial learning (Yang and Lisberger, 2014). Voltage states or simple spike firing rates (SSFRs) (well known to represent voltage states *in vitro* and recently demonstrated *in vivo* [Jelitali et al., 2016]) have been correlated with CS spikelet numbers in some studies (Burroughs et al., 2017; Gilbert, 1976; Khaliq and Raman, 2005; Monsivais et al., 2005), but not in others (Mano, 1970; Warnaar et al., 2015). Additionally, CSs can be modulated by CF firing rates (FRs), but contradictory correlations between spikelet numbers and the instantaneous CF FRs have been reported (Burroughs et al., 2017; Khaliq and Raman, 2005; Maruta et al., 2007; Warnaar et al., 2015). Thus, it is necessary to re-examine how the CS shape is regulated.

Spiking is energetically expensive (Attwell and Laughlin, 2001). Each CS consumes more energy than a simple spike (SS), but neither can be measured experimentally.

To address these questions, a systematic exploration of CF responses with high spatiotemporal resolution is required. Given the difficulty of simultaneously recording at numerous locations in the same cell by patch clamp (Davie et al., 2008; Stuart and Häusser, 1994) and the lack of direct spike information from Ca^{2+} imaging (Deneux et al., 2016), computer models can play an indispensable role. Here, we have built a “canonical” PC model that reproduces most available experimental observations instead of fitting it to a specific cell recording. We use this model to systematically explore factors that affect CF-evoked dendritic and somatic responses and estimate the energy consumed for SSSs and CSs.



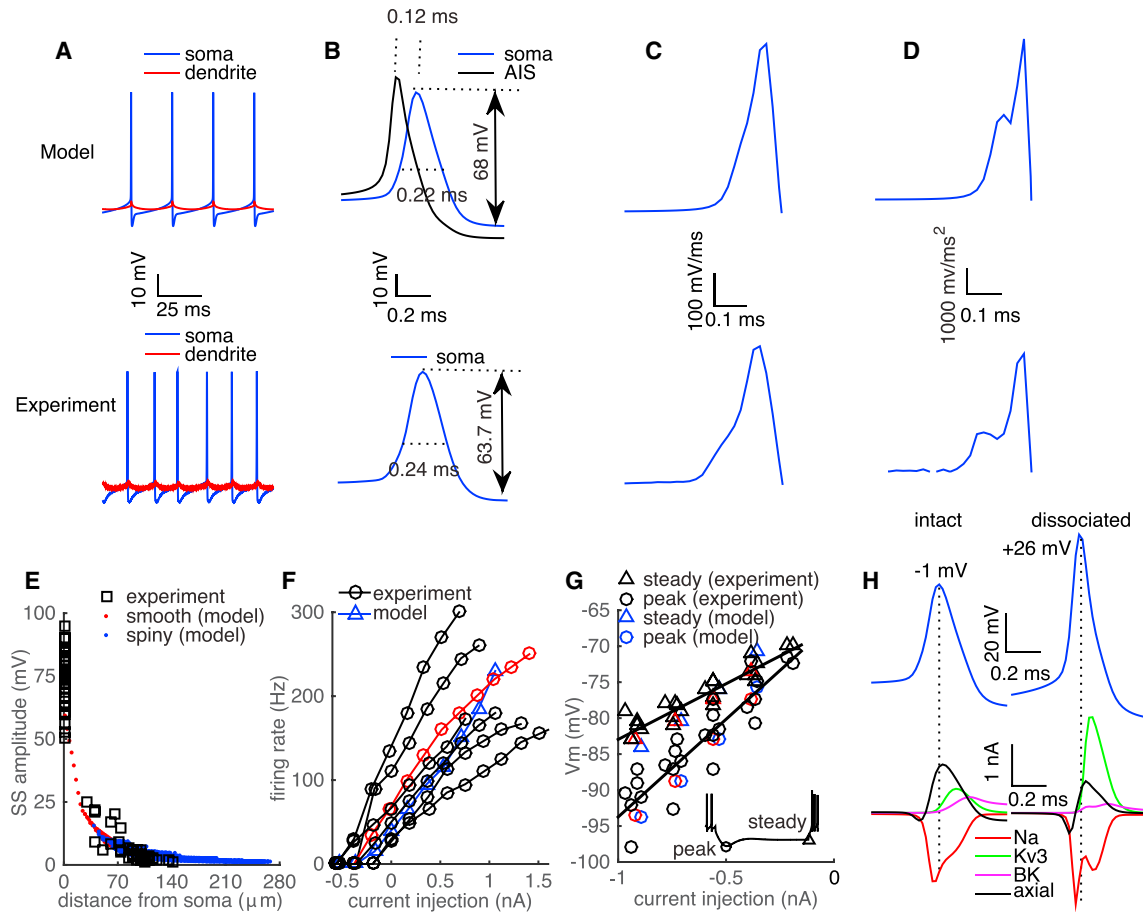


Figure 1. Model Properties Compare Well with Experimental Data

(A) Spontaneously firing SSs and dendritic membrane potentials (103 μm from soma) from the model and experiments (dendritic site is ~ 100 μm from soma). (B) A single SS from the model and experiments. The spike at the AIS is aligned to measure the axosomatic delay in the model. (C and D) The dv/dt and d^2v/dt^2 of the SS in the model are compared with experimental data in (C) and (D) separately. (E) Distance-dependent decay of SS amplitudes in the model and experimental data (Ohtsuki et al., 2012). (F) The F-I curve of the model compared with experimental data. (G) The peak and steady-state values of sag responses caused by negative current injections are compared between model and experimental data. In (F) and (G), red symbols are from the example cell used in (A)–(D). The data used in (A)–(D), (F), and (G) are from Rancz and Häusser (2010). (H) Distinct spike peaks and principal ionic current profiles in the intact and the dissociated PC model. In the dissociated PC, only the dendritic root section before the first bifurcation is preserved. Ionic currents are computed at the central segment (surface area of 204 μm^2) of the soma.

RESULTS

Electrophysiological Properties of SSs

Before using the model to make predictions, we first compare its basic properties with *in vitro* experimental data. Example cell recordings are shown in Figures 1A–1D to help the comparison. Our PC model spontaneously fires at 40 Hz in the absence of synaptic inputs or current injections (27–140 Hz in experiments). SSs initiate first at the axon initial segment (AIS) with an axosomatic delay of 0.12 ms (~ 0.1 ms reported by Palmer et al., 2010). The SS peak is -1 mV and its amplitude is 68 mV (-11 to -3 mV and 56 to 68 mV, respectively, in experiments). SSs have a half-amplitude duration of 0.22 ms (0.22–0.28 ms in experiments). The peak dv/dt of SSs is 530 mV/ms (440–540 mV/ms in experiments). The d^2v/dt^2 of SSs shows a

biphasic increase, with the first component reflecting the contribution of axial current from the AIS and the second one reflecting the contribution of somatic Na^+ current. The peak value of d^2v/dt^2 is 6,600 mV/ms² (5,600–8,200 mV/ms² in experiments).

Due to the absence of dendritic Na^+ channels (Stuart and Häusser, 1994) and the large impedance load of elaborate dendritic trees (Vetter et al., 2001), SSs fail to invade the dendritic tree (Linás and Sugimori, 1980). The distance-dependent decay of SS amplitudes in the model matches experimental data (Figure 1E; also close to Stuart and Häusser, 1994). The model also performs well in response to somatic current injections. The F-I curve falls within the experimentally measured range (Figure 1F). Similar to that of Fernandez et al. (2007), our model has type I excitability. When a large enough negative current is

injected, the cell is silenced and shows a typical “sag” response (illustrated in the inset of Figure 1G). Both the peak and steady state of the sag response are within the range of experimental data (Figure 1G). This good overall performance in response to current injections suggests that the model is reliable in predicting excitatory and inhibitory synaptic responses in PCs.

Dissociated PCs are often used to investigate the role of ionic currents in PC electrophysiological properties (Carter and Bean, 2009; Khaliq et al., 2003; Swensen and Bean, 2003). However, we find the profiles of Na⁺ current (principal depolarization current [Carter and Bean, 2009]) and of Kv3 current (principal repolarization current [Martina et al., 2007]) in an intact PC strongly differ from in a dissociated PC owing to their distinct spike properties (Figure 1H). Similar to that of Bekkers and Häusser (2007), the intact PC model exhibits a higher spike threshold, smaller afterhyperpolarization, and lower spike peak compared with the dissociated PC. The lower spike peak (−1 mV in the model) compared with the dissociated PC (+26 mV in the model, +32 mV in Carter and Bean, 2011, and ~+40 mV in Bekkers and Häusser, 2007) leads to a much smaller fraction of Kv3 channels activated, due to their high activation threshold (Martina et al., 2007). In the intact PC, the dendrite repolarizes somatic SSs together with the “less” activated Kv3 current. This large axial current (flow into dendrite) keeps pace with SS depolarization to constrain its peak to −1 mV (a smaller axial current exists in the dissociated PC due to the remaining dendritic stump). At the peak of the spike, the “dip” in the Na⁺ current observed in dissociated PCs (Carter and Bean, 2009) is absent in the intact PC model.

The Na⁺ entry ratio (the ratio of total Na⁺ influx to the Na⁺ influx during the rising phase [Carter and Bean, 2009]) can decrease from 3.0 in the dissociated PC model to 2.2 in the intact PC model. Although dendrites lack Na⁺ channels, SSs passively propagate into dendrites and partially activate Ca²⁺ channels in proximal dendrites. Therefore, we compute the ATP molecules required for each SS to better understand their energy consumption (Attwell and Laughlin, 2001). In our model, 4.3×10^7 ATP molecules are required to pump Na⁺ ions and Ca²⁺ ions out of the PC after a SS, with 60% of the energy expended on Na⁺ ions.

CF Responses in the PC

When PCs receive synaptic inputs from CFs, stereotypical CSs occur at their somas. CF responses at different sites of a spontaneously firing PC model are shown in Figure 2A. The peak dv/dt of the first spikelet in the CS is ~270 mV/ms larger than that of the SS, as confirmed by *in vitro* experimental data (Figure 2B). The large peak dv/dt of the first spikelet ensures its reliable propagation down to the cerebellar nuclei (CN) (Khaliq and Raman, 2005; Monsivais et al., 2005). The CS still initiates first at the AIS (Palmer et al., 2010) with an axosomatic delay of the first spikelet of 0.06 ms, which is much shorter than that of the SS (Figure 2C). This decreased axosomatic delay is caused by the depolarizing CF excitatory postsynaptic current (EPSC) during the initial depolarization phase (Figure 2D). The model also replicates varied CF responses due to bursting CF input (Mathy et al., 2009) (Figure S1).

In agreement with previous experimental findings (Swensen and Bean, 2003), the SK2 current terminates the CS (Figure 2D).

Each spikelet of the somatic CS in our model, except the last one, is sharp (Figure 2A), suggesting they are generated by Na⁺ channels (Figure 2D). Two factors determine the absence of Ca²⁺ spikes at the soma. First, the P-type Ca²⁺ current is much smaller than the Na⁺ current; therefore, the Na⁺ current shunts it. Second, K⁺ currents are always larger than the P-type Ca²⁺ current (Figure 2D). Magnitudes of the CF EPSC and the net axial current are comparable to somatic ionic currents (Figure 2D), suggesting an important role in generating somatic CSs. Consequently, a variation of either CF EPSC or axial current has the potential to alter somatic CSs, as shown in later sections.

The dendritic root section (the section between the soma and the first dendritic bifurcation) is electrically compact with the soma and shows mainly a passive propagation of a somatic CS. With distance from the soma, the clamping effect of the somatic CS on the dendrite weakens. The P-type Ca²⁺ current gradually dominates and causes Ca²⁺-driven dendritic responses in the PC dendrite (Figures 2A, 2E, and 2F).

Factors Regulating the Initiation and Propagation of Dendritic Spikes

Here, we systematically explore how different voltage states, caused by varying the somatic holding current, regulate CF-evoked dendritic responses and analyze the biophysical mechanisms. We find depolarization facilitates higher peaks of dendritic responses with further propagation into distal spiny dendrites. In distal spiny dendrites, axial currents from proximal smooth dendrites are the only current sources that can depolarize to approach the Ca²⁺ spike threshold and trigger a dendritic spike (Figures 3J–3L). When the soma is held at −76 mV (Figure 3A), the A-type Kv4 current is larger than the P-type Ca²⁺ current in spiny dendrites (Figure 3J). Consequently, axial currents cause only small passive depolarizations in spiny dendrites (Figure 3D), and P-type Ca²⁺ channels are hardly activated (Figure 3J). In smooth dendrites, the CF provides powerful synaptic input to depolarize (Figure 3D). However, this depolarization is still passive because the Kv4 current and axial currents (flow into distal parts) stop the P-type Ca²⁺ current from dominating depolarization (Figure 3M). Accordingly, the dendritic voltage responses decrease with distance from the soma in the whole dendrite (Figure 3G). Distance-dependent propagation of voltage responses matches experimental recordings under the same conditions (Figure 3G). As the soma is held at −70 mV (Figure 3B), dendritic spikes occur in part of the dendritic tree (the left half, proximal to the soma), where the voltage responses now increase with distance from the soma. However, the responses still decay with distance from the soma in other parts of the dendritic tree (Figures 3B, 3E, and 3H). With depolarization of the soma to −61 mV (Figure 3C), the Kv4 current gradually inactivates and becomes smaller than the P-type Ca²⁺ current in both smooth and spiny dendrites during the initial depolarization phase (Figures 3L and 3O). As a result, the P-type Ca²⁺ current depolarizes the dendrites and activates more Ca²⁺ channels in a positive-feedback loop until the Kv3 current is highly activated to repolarize the spikes. Dendritic spikes occur globally and their peaks increase with distance from the soma (Figures 3F and 3I). In line with voltage responses, the

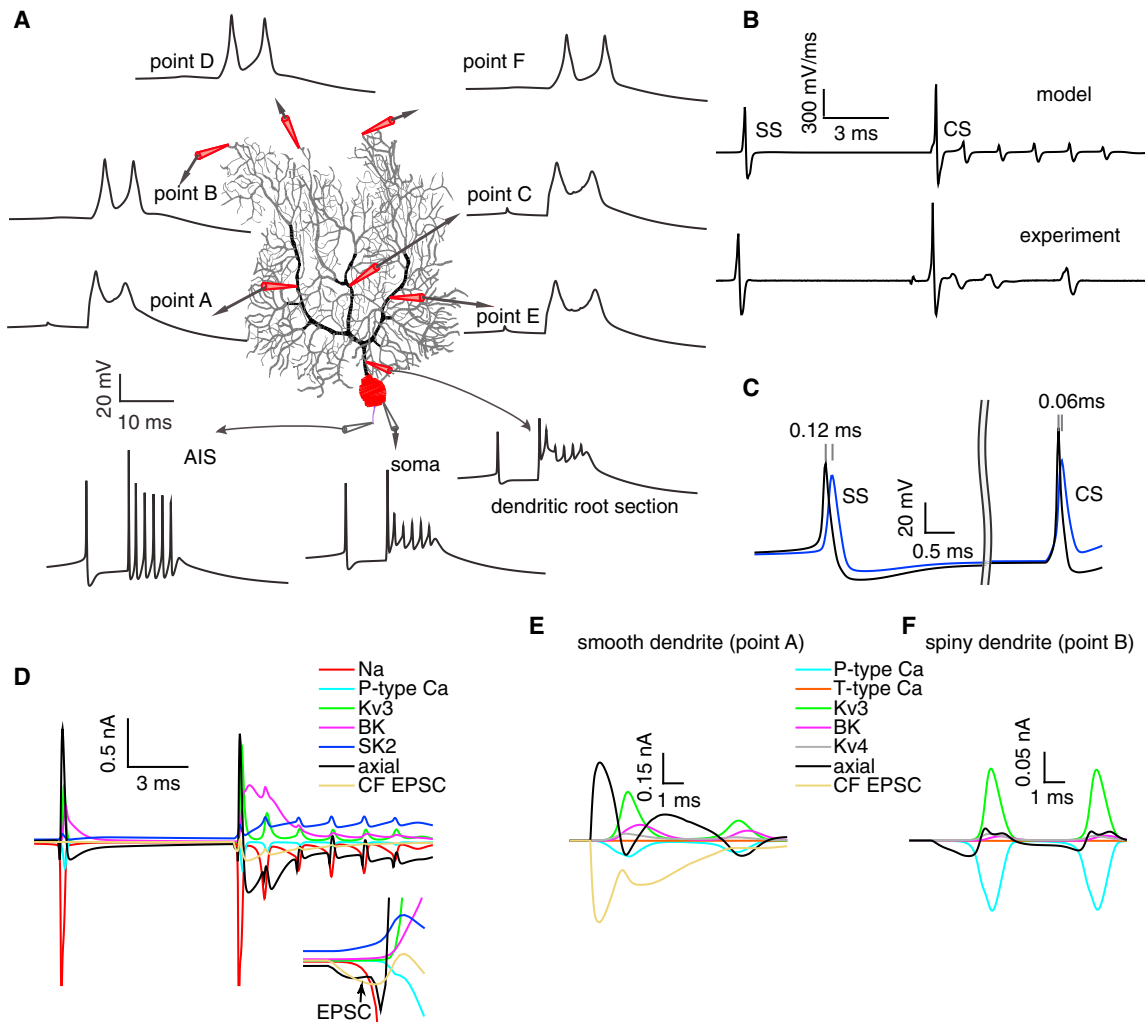


Figure 2. The Generation of CF Responses in the PC

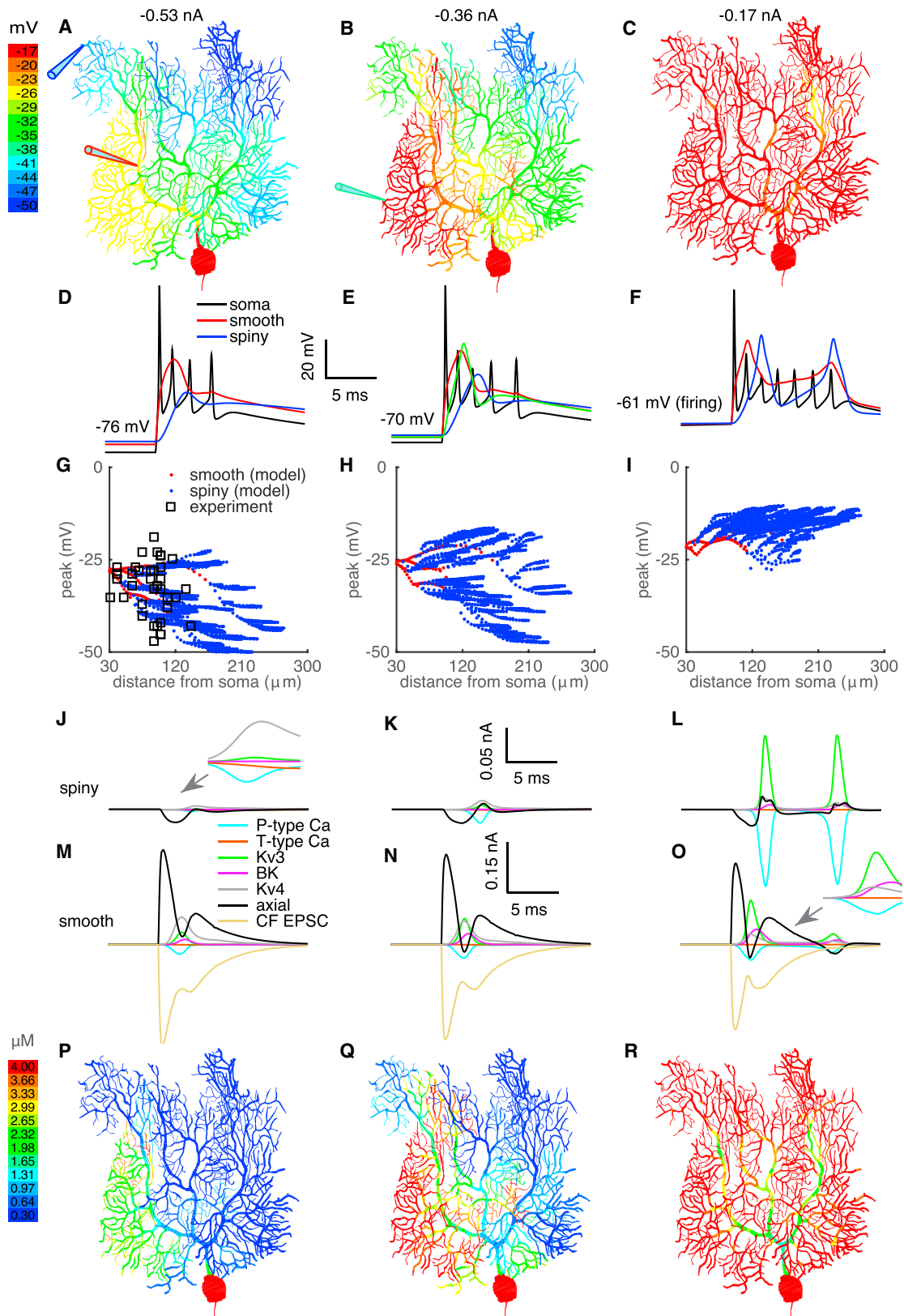
(A) CF responses at different sites in the PC model. Two sites on each main branch are selected. Points A (smooth dendrite) and B (spiny dendrite) on branch 1; points C and D on branch 2; points E and F on branch 3. CF responses at dendritic root section, soma, and AIS are labeled by corresponding arrows. (B) The peak dv/dt of the first CS spikelet increases compared with a SS in both model and experiment (Warnaar et al., 2015). (C) The axosomatic delay of the first spikelet in the CS decreases compared with a SS. (D) The composition of the somatic CS. Currents at the initial depolarization phase are enlarged in the inset. (E and F) Dendritic currents at points A and B are shown in (E) and (F) in sequence. The surface areas of the segments chosen at the soma, point A, and point B are 204, 64, and 23 μm^2 , respectively. CF EPSC is absent in the spiny dendrite. Notice different scales used in (D)–(F) due to different segment surface areas.

dendritic Ca^{2+} influx is also facilitated by depolarization, causing larger and more widespread elevations in dendritic Ca^{2+} concentration (Figures 3P–3R). Additional CF responses at other voltage states are shown in Figure S2.

The critical role of Kv4 current in regulating dendritic spike propagation is further demonstrated in Figure S3. After blocking dendritic Kv4 current, dendritic spikes reliably propagate to the whole dendrite at more hyperpolarized conditions. We further test whether other K^+ currents regulate the propagation of CF-evoked dendritic response. Blocking the high-threshold-activated Kv3 current surprisingly facilitates the propagation of dendritic spikes (Figure S4) (Otsu et al., 2014; Zagha et al., 2010). Unlike the “brake” mechanism of Kv4 current, dendritic

Kv3 current mainly narrows the CF response and only activates when the response is large enough (Figures 3J–3O). Blocking the Kv3 current broadens the dendritic responses at smooth dendrites and facilitates their propagation to spiny dendrites. The effect of broadening dendritic responses on their propagation is further demonstrated in Figure S5. Dendritic BK current does not significantly affect the propagation of CF-evoked dendritic responses (data not shown).

Taken together, these results suggest that availability of dendritic K^+ channels not only regulates the amplitude (Kitamura and Häusser, 2011; Rokni et al., 2009) but also gates the spatial range of Ca^{2+} influx (Ohtsuki et al., 2012; Otsu et al., 2014; Zagha et al., 2010). Voltage conditions can also explain the distinct



(legend on next page)

dendritic spike waveforms recorded *in vitro* by different groups (Davie et al., 2008; Ohtsuki et al., 2012) in Figure S6.

Inhomogeneous Excitability of the Dendritic Tree

Similar to the first dendritic spikelet (Figure 3B), the secondary dendritic spikelet occurs asynchronously in different branches around its threshold (Figure 4). It initially occurs at branch 1; then it gradually occurs at branch 2 and finally occurs at branch 3 with slightly increasing depolarization. Even when secondary dendritic spikelets occur globally, their time to peak still differs between branches (Figure 4C). They peak at 8.36, 10.74, and 13.64 ms at points A, C, and E, respectively (relative to CF activation time). With further depolarization, secondary dendritic spikelets peak more synchronously (with 0.89-nA current injection, the respective values become 6.06, 6.88, and 7.32 ms). The asynchronous occurrence of individual spikelets reflects the inhomogeneous excitability of each dendritic branch. In the model, the density of ionic currents is homogeneous in the spiny dendritic tree. Therefore, morphological differences between individual branches may account for heterogeneous excitability. The excitability of each branch is determined by the ratio of spiny dendrite area to smooth dendrite length in that branch (essentially the ratio of spiny dendrite capacitance load to CF synaptic input, “load/input” ratio; [Experimental Procedures](#)). The load/input ratios are 69, 96, and 131 at branches 1, 2, and 3, respectively, explaining their heterogeneous excitability. Moreover, within each “big” branch, “small” child branchlets also show heterogeneity in excitability (Figures 3A–3C), which are caused by other morphological factors such as the electrotonic distance to smooth dendrites.

K⁺ currents activated near “resting” dendritic membrane potentials may enhance the heterogeneous excitability. The whole dendrite becomes more homogeneous at hyperpolarized levels after blocking the Kv4 current (Figure S3). Essentially, uneven distributed load/input ratios underlie the heterogeneous dendritic excitability, but dendritic Kv4 channels enhance it.

Voltage- and Phase-Dependent Somatic CSs

Similar with dendritic responses, somatic CSs also vary significantly with depolarization (Figures 5A–5C). The spikelet numbers in CSs increase with initial depolarization, but decrease with further depolarization. A somatic CS results from the interaction of intrinsic ionic currents, axial current, and CF EPSC (Figure 2D). At low voltage, although Na⁺ channel availability decreases slightly (Figure 5C), increased axial current from larger dendritic responses (Figure 5A) dominates and triggers more somatic spikelets. Interestingly, the largest number of somatic spikelets coincides with the longest occurrence latency of secondary den-

drolic spikelets (Figure 5A). With further depolarization, Na⁺ channel availability decreases at a higher rate (Figure 5C). Also, secondary dendritic spikelets peak faster and closer to a preceding somatic spikelet (Figure 5A). The shortened interval between secondary dendritic spikelets and their preceding somatic spikelet means fewer Na⁺ channels are recovered to evoke an extra somatic spikelet (right axis of Figure 5D). The critical role of secondary dendritic spikelet timing in evoking an extra somatic spikelet agrees with previous experimental observations (Davie et al., 2008). Both factors decrease somatic spikelets with further depolarization. Concurrent with spikelet numbers, CS durations are regulated by voltage states, as represented by the timing of the last spikelets (Figure 5B).

With depolarization, the consumed ATP molecules during CSs increase from 1.1×10^8 (–84 mV) to 1.5×10^9 for a CS with two dendritic spikelets (nearly 40 times as large as in a SS), with 96% of the energy expended on Ca²⁺ ions (Figure 5A). The increased ATP consumption with depolarization is due to increased Ca²⁺ influx (Figures 3, 5A, and S2), but relatively insensitive to somatic spikelet variations.

Voltage states also affect spikelet amplitudes in CSs. We analyzed the first three spikelets, which exist in all simulated voltage conditions. Spikelet amplitudes decrease with depolarization due to reduced availability of Na⁺ channels (Figure 5C). Individual spikelet amplitude is critical because it determines the probability of propagation down to the CN (Khaliq and Raman, 2005; Monsivais et al., 2005).

Finally, we observed phase dependency of somatic CSs. Amplitudes of the first two spikelets in CSs decrease and the spikelets become more blunted with shortening of the interval between the CF activation and its preceding SS (Figure 5D). This phase dependency reflects the time course of Na⁺ channel recovery from inactivation. We confirmed this phase dependency by reanalyzing *in vitro* experimental recordings.

So far, voltage states of the PC model were manipulated by varying somatic holding currents. We implemented more realistic *in vivo* simulations (Jelitali et al., 2016), in which the net balance of excitatory PF and inhibitory synaptic inputs determines the dendritic voltage states (Figure S7). We find that the effect of voltage states on CF responses found *in vitro* also holds *in vivo*. We also analyze pauses following CSs (data *in vitro* not shown) and find their durations decrease with depolarization in our model (Figure S7I), due to the larger depolarization force.

Spatially Constrained Modulation by Clustered PF/ Stellate Cell Synaptic Input

Sensory stimuli can activate clustered PF synaptic inputs (Wilms and Häusser, 2015). Here, we examine how simultaneous

Figure 3. Voltage States Regulate CF-Evoked Dendritic Spike Generation and Propagation

From left to right column, the holding potentials are –76, –70, and –60 mV, respectively.

(A–C) Color-coded voltage responses with depolarization.

(D–F) Somatic CSs, voltage responses on the smooth dendrite and spiny dendrite with depolarization. In (E), an extra example voltage response (green trace, position indicated in [B]) on the spiny dendrite is shown.

(G–I) Distance-dependent propagation of voltage responses with depolarization. Experimental data in (G) are from Ohtsuki et al. (2012).

(J–O) Ionic currents in the spiny dendrite (J–L) and smooth dendrite (M–O), respectively, with depolarization. The surface areas of the segments chosen at the smooth dendrite and spiny dendrite are 64 and 23 μm^2 , respectively.

(P–R) Color-coded Ca²⁺ concentrations with depolarization.

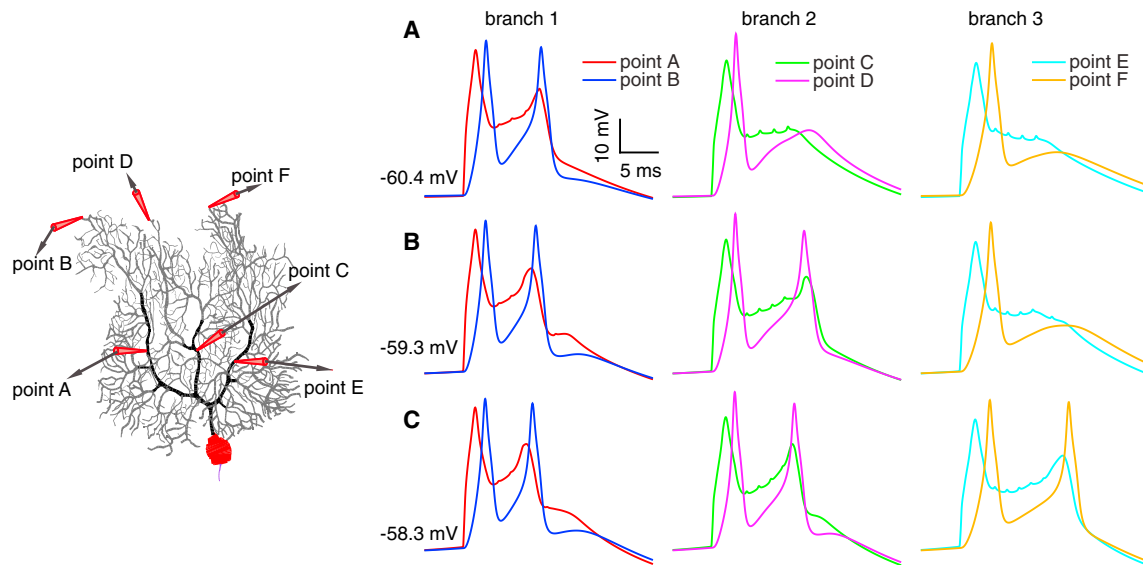


Figure 4. Branch-Specific Occurrence of Secondary Dendritic Spikelets

(A–C) In all simulations, the holding current is -0.17 nA. CF input is activated at three slightly different dendritic voltage states (different phases of somatic interspike intervals) as shown in (A), (B), and (C).

clustered PF or stellate cell synaptic inputs regulate CF responses. We find that clustered synaptic inputs regulate dendritic responses in a spatially constrained manner. A secondary dendritic spikelet only occurs at branch 1 with CF input in isolation (Figure 6A). With five PF synapses simultaneously activated at the indicated branchlet of branch 2, the secondary dendritic spikelet also occurs at this branchlet. Concurrently, an extra spikelet is evoked in the somatic CS. Nonetheless, clustered PF synaptic inputs within branch 2 do not significantly affect other branches. Seemingly paradoxically, the extra somatic spikelet is eliminated if the number of simultaneously activated PF synapses increases to 20. As explained previously, Na^+ channels need time to recover from inactivation after each somatic spikelet. Increasing PF synaptic inputs accelerates secondary dendritic spikelets, making them occur closer to the preceding somatic spikelet, and reducing the likelihood of triggering an extra spikelet due to fewer recovered Na^+ channels. Similarly, simultaneous activation of ten stellate cell synaptic inputs can evoke an extra somatic spikelet by delaying the secondary dendritic spikelets at branch 2 (Figure 6B). Again, dendritic responses at other branches are minimally affected. The secondary dendritic spikelet still occurs in the proximal smooth dendrite even when it is eliminated in the distal part by activating 20 stellate cell synaptic inputs.

We also show that compartment-specific dendritic excitability (Ohtsuki et al., 2012), simulated by regional Kv4 block, modulates dendritic responses in a spatially precise way (Figure S8).

Paired-Pulse Depression Regulates CF Responses in the PC

CFs can transiently fire at ~ 5 – 8 Hz after sensory stimuli (Najafi et al., 2014; Warnaar et al., 2015). Paired-pulse depression (PPD) has been demonstrated for consecutive CF synaptic

inputs *in vitro* (Andjus et al., 2005; Hansel and Linden, 2000), and it may support the correlation between instantaneous CF FRs and varied CS spikelet numbers. To investigate the effect of PPD on CF responses, we systematically explore CF responses with baseline or 20% depressed CF EPSC (~ 4 Hz of instantaneous CF FR in experiments by Andjus et al., 2005). We find depressed CF inputs consistently reduce dendritic responses. At low voltage, the peak of the dendritic response decreases (Figure 7A); at higher voltage, the appearance of a secondary dendritic spikelet is prevented (Figure 7B) or delayed (Figure 7C). The spikelet numbers in somatic CSs show no changes, decreases, or increases with depressed CF inputs at different voltages (Figures 7A–7C). A depressed CF input always delays individual somatic spikelets by providing less depolarization current. At low voltage, 20% depression of the CF EPSC and slightly reduced dendritic response are insufficient to vary somatic spikelet number and only increase CS duration (Figure 7A and case I in Figure 7D). At medium voltage, baseline CF input evokes a secondary dendritic spikelet. The increased axial current (the later stage of ionic currents in Figure 7B) triggers extra somatic spikelets due to the relatively large availability of Na^+ channels (see Na^+ current amplitude). Therefore, by failing to cause a secondary dendritic spikelet, depressed CF input decreases CS duration because of fewer somatic spikelets, although they are delayed (Figure 7B and case II in Figure 7D). At high voltage, depressed CF input delays individual spikelets and allows for larger recovery of Na^+ channels. The delayed secondary dendritic spikelet also facilitates occurrence of extra somatic spikelets. Thus, depressed CF input increases CS duration (Figure 7C and case III in Figure 7D).

Voltage ranges for the occurrence of cases I–III depend on the degree of depression. For example, when CF EPSC is depressed

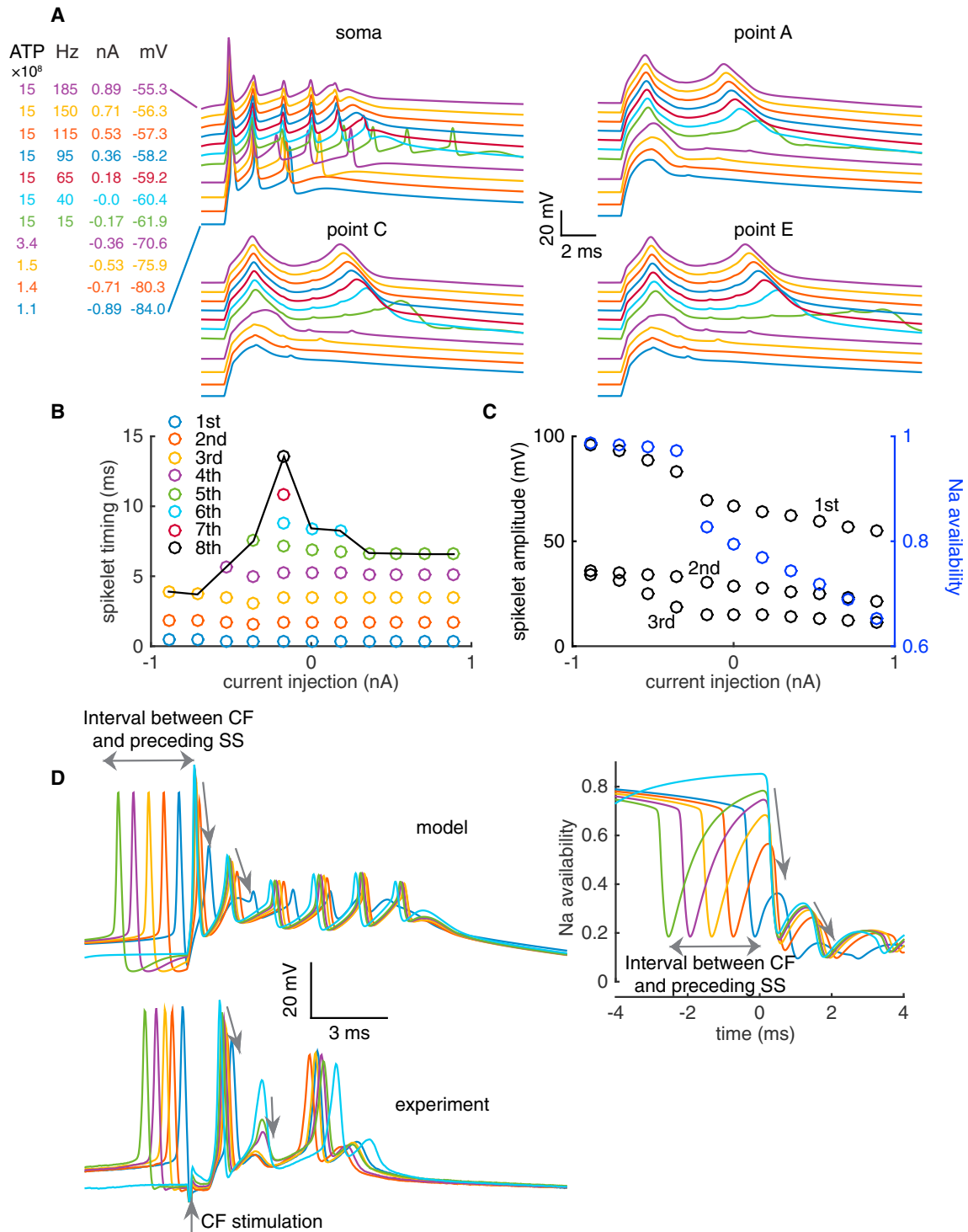


Figure 5. Voltage- and Phase-Dependent Somatic CSs

(A) Voltage states affect somatic CSs and corresponding dendritic responses. The definition of dendritic sites is the same as in Figure 2. The holding currents, the FRs, and the consumed ATP molecules at each voltage state are listed on the left.

(B) Voltage states modulate CS durations, represented by the timing of the last spikelets.

(C) In parallel with Na^+ channels availability (blue circles), amplitudes of the first three spikelets in the CS (black circles) decrease with depolarization.

(D) Amplitudes of the first and second spikelets are phase dependent in model and experiments (Warnaar et al., 2015). Phase-dependent recovery of Na^+ channels is shown in upper right panel.

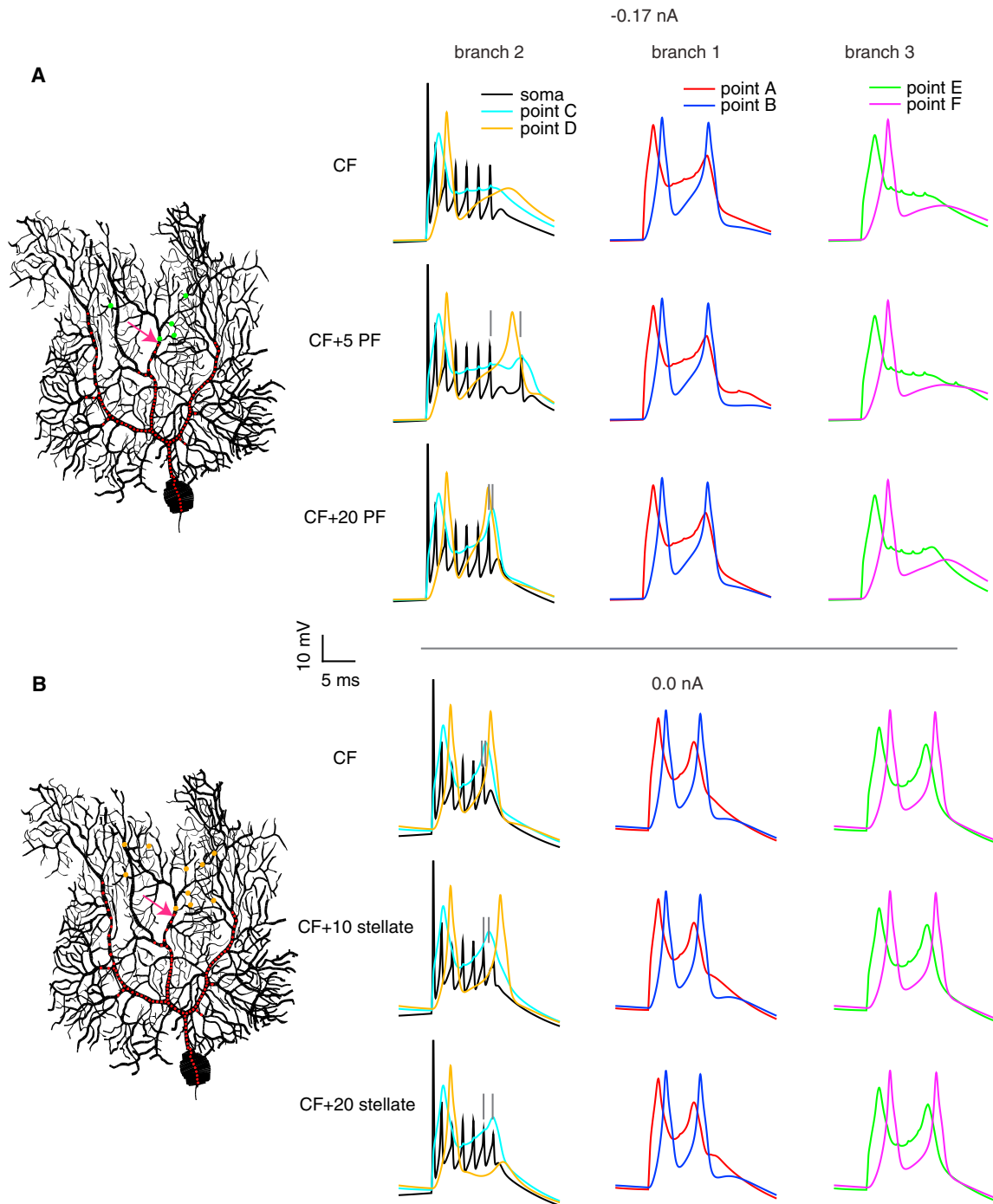


Figure 6. Simultaneous Clustered PF or Stellate Cell Synaptic Input Regulates the CF-Evoked Somatic CSs by Locally Modulating the Dendritic Responses

(A) Somatic and dendritic responses with only CF input (red dots), CF input + 5 PF synaptic inputs, and CF input + 20 PF synaptic inputs are shown from top to bottom. PF synapses are randomly distributed on the indicated dendritic child branchlet (green dots).

(B) Somatic and dendritic responses with only CF input, CF input + 10 stellate cell synaptic inputs, and CF input + 20 stellate cell synaptic inputs are shown from top to bottom. Similar placement of stellate cell synapses (orange dots). The definition of recorded dendritic sites is the same as in [Figure 2](#).

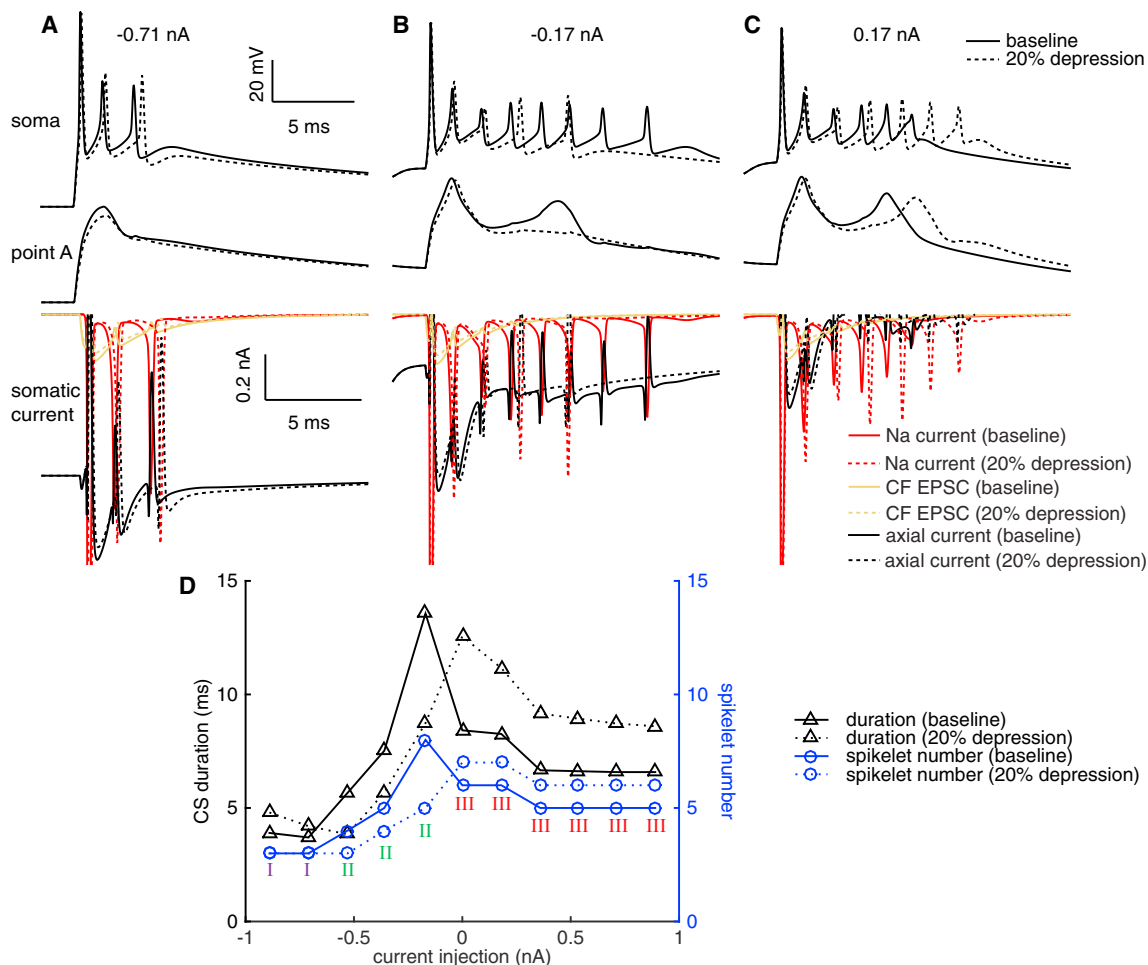


Figure 7. PPD Regulates CF Responses

(A–C) CF responses (somatic and dendritic) and somatic ionic currents with unchanged (case I), decreased (case II), and increased (case III) spikelet numbers per CS by depressed CF EPSC are shown in (A), (B), and (C) in sequence. Ionic currents are computed in the central segment of the soma, and Na⁺ currents during the first spikelet are truncated.

(D) The effect of depressed CF EPSC on the spikelet number and duration of the CSs.

by 10%, case I can occur at both low and high voltages (data not shown). Also, when CF FRs are higher, incomplete recovery of ionic currents from preceding CS such as SK2 and the dendritic hyperpolarization may vary the posterior CS in a more complicated way.

Thus, PPD can bridge the gap between instantaneous CF FRs and CS variations. Our results reconcile the observed unchanged (Warnaar et al., 2015), decreased (Khaliq and Raman, 2005; Maruta et al., 2007), and increased (Burroughs et al., 2017) somatic spikelet numbers at higher CF FRs.

DISCUSSION

We built a new PC model based on extensive experimental data to systematically investigate CF responses. Simulation results help to reveal the mechanisms causing spikes on different parts of PCs, reconcile conflicting experimental data, and make new predictions.

Model Accuracy

We constrained model parameters by hand tuning and tried to replicate as many experimental observations as possible. We started by constraining somatic ionic currents based on ionic current measurements taken from dissociated PCs. These data allowed us to uniquely constrain principal somatic currents. Subsequently, the ionic currents in the AIS and dendrites were constrained to obtain the spike properties summarized in Figure 1. It was more difficult to constrain dendritic ionic currents due to insufficient data. The total Ca²⁺ influx during one dendritic spikelet was constrained by the experimentally estimated value. In addition, the replicated CF-evoked dendritic responses under different conditions (Figures 3, S2, S4, and S6) suggest that the dendrite model produces realistic results. Nonetheless, there is still room for improvement in the future. Due to the lack of specific data, we did not try to reproduce the role of dendritic SK2 current (Ohtsuki et al., 2012; Womack and Khodakhah, 2003) and Kv1 current (Khavandgar et al., 2005) in regulating dendritic

excitability. These currents may further enhance the heterogeneous excitability and regulate dendritic responses. The data we used to directly validate our simulation results are all from *in vitro*. We hope our study will inspire experiments to validate modifiable CF responses *in vivo*.

Our PC model follows the tradition of the biophysical modeling by De Schutter and Bower (1994a, 1994b), which has successfully predicted experimental findings (Steuber et al., 2007). Although the 1994 model is outdated by recent knowledge of ionic channels in PCs, there was no suitable replacement until now. A PC model by Khaliq et al. (2003) has no dendrite and therefore cannot be used to simulate synaptic responses. A recent PC model (Masoli et al., 2015) lacks extensive validation against experimental data.

Physiological Predictions and Implications

The model allows us to predict the metabolic cost of spiking in PCs. In a cortical pyramidal neuron, $\sim 4 \times 10^8$ ATP molecules are consumed to restore the Na^+ and K^+ ion gradients after each spike (Attwell and Laughlin, 2001). Carter and Bean (2009) reported that spiking is energetically less efficient in PCs compared with cortical pyramidal neurons. However, their study was performed in dissociated PCs. We find the intact PC has a smaller Na^+ entry ratio compared with the dissociated PC (Figure 1H), suggesting that dendrites increase the metabolic efficiency of somatic spikes. Given the energetic cost of spikes, it will be interesting to explore whether this dendritic role also applies to other neurons. Compared with Na^+ entry ratio, the estimated energy consumption may be a better measure because of the Ca^{2+} channels distributed in soma, axon, and elaborate dendritic tree. Interestingly, although cortical pyramidal neurons have a low Na^+ entry ratio (~ 1.1 by Carter and Bean, 2009), their estimated energetic cost of a single spike is approximately eight times larger than a SS in PCs, due to the lack of Na^+ channels in PC dendrites. Each CS consumes more ATP molecules, which consumes nearly the same amount of energy as 40 SSs during 1 s in our model. Possibly, previously reported negative correlation (Cerinara and Rawson, 2004) between the FRs of SSs and CSs may be a protective mechanism given the limited energy supply in the cerebellum.

CF-evoked dendritic spikes and somatic CSs are generated by different channels intrinsically, but they communicate via axial currents through the dendritic root section (Figure 2). Due to technical challenges, dendritic patch-clamp recording is usually performed on smooth dendrites of large diameter. Although we could reproduce the experiment by Davie et al. (2008) in the model (Figure S9), we show that a single-site dendritic recording cannot reliably reflect spike occurrence and propagation in the whole dendrite. Both the peak and occurrence latency of secondary dendritic spikelets can be modulated. The peak of secondary dendritic spikelets decreases in the somatopetal direction due to unevenly distributed impedances (Roth and Häusser, 2001; Vetter et al., 2001) and K^+ channels (Martina et al., 2003). When a secondary dendritic spikelet is “weak,” with small amplitude and long latency, it may fail to trigger a regenerative dendritic spike in proximal dendrites (branch 1 in Figure S9). Therefore, the role of dendritic spikes in evoking extra somatic spikelets may have been underestimated.

Using the model, we deciphered how voltage-dependent K^+ currents regulate the amplitude (Kitamura and Häusser, 2011; Rokni et al., 2009) and spatial range of Ca^{2+} influx (Figures 3, S2–S4, and S7) as observed in separate experiments (Ohtsuki et al., 2012; Otsu et al., 2014; Zagha et al., 2010). Vetter et al. (2001) have explored the local propagation of dendritic spikes by exerting an AP clamp at a specific dendritic site. We find that dendritic spikes on the smooth dendrite can overcome the impedance mismatch and propagate to distal dendrites in the absence of the brake role of Kv4 in distal dendrites (Figures S3 and S5). Therefore, K^+ currents activated around the “resting” dendritic membrane potential such as Kv4 in spiny dendrites are necessary to gate the spatial range of CF-evoked dendritic responses. Unlike Kv4 current, Kv3 current narrows the dendritic response to regulate its propagation (Figures S4 and S5). The voltage-related amplitude and spatial range of dendritic responses indicate that PCs can play active roles in response to CF error signals rather than passively accepting instruction from their CF “teachers.” PF synapses can undergo not only long-term depression (LTD) (with a higher Ca^{2+} -induction threshold) but also long-term potentiation (LTP) (with a lower Ca^{2+} -induction threshold) (Coesmans et al., 2004; Gallimore et al., 2018; Piochon et al., 2016). The voltage-regulated dendritic spike amplitude and spatial range suggest that CF may trigger LTP, a mixture of regional LTP and LTD, or LTD depending on the voltage states of PCs. Such effects will be further modified by stochastic gating of Ca^{2+} and K^+ channels (Anwar et al., 2013), which was not simulated in this study.

The PC dendritic tree exhibits inhomogeneous excitability in individual branches, implying a computational unit at the level of individual branches, or even smaller branchlets (Figure 4). Building upon the modulated voltage states of PCs, branch-specific computation can undoubtedly increase the capacity of information processing in PC dendrites, in contrast to the traditional view of the whole dendrite as the computational unit of CF response. Notably, branchlet-specific Ca^{2+} influx has been demonstrated for PF synaptic integration (Wang et al., 2000). When PCs receive concurrent clustered synaptic input (Wilms and Häusser, 2015) or undergo localized dendritic excitability plasticity (Ohtsuki et al., 2012), CF-evoked dendritic responses can be modulated more precisely in space and magnitude to affect the plasticity induction (Figures 6 and S8).

CS shapes are quite variable. In our model, we did not get the small second spikelets as observed in some experiments (Davie et al., 2008; Monsivais et al., 2005), but our CS shapes are close to other recordings (Jelitai et al., 2016; Mathy et al., 2009; Otsu et al., 2014). We speculate that CS shapes are cell dependent. Recently, CS durations have been linked to the degree of trial-over-trial learning (Yang and Lisberger, 2014), with the mechanism underlying variable CSs unresolved. The authors assumed that the variation of CS durations is due to the bursting of CF inputs, based on Mathy et al. (2009). We correlate the spikelet numbers and durations of CSs with voltage states or SSFRs (Figures 5A and 5B). Besides reconciling previous contradictory correlations between spikelet numbers and SSFRs (Bourgeois et al., 2017; Gilbert, 1976; Khaliq and Raman, 2005; Mano, 1970; Warnaar et al., 2015), our results provide an

alternative interpretation of the work by Yang and Lisberger (2014). Our interpretation highlights the importance of all synaptic inputs to the PCs and resulting SSFRs, not just CF, to control learning. Additionally, the CS spikelet amplitudes can be modulated by voltage states (Figures 5C and S7H). The timing of CF activation (phase dependency) and concurrent synaptic input also affect somatic CSs (Figures 5D and 6). All of these factors vary CS shapes and may modulate the PC output and affect inhibition of the CN. Although CF-evoked pause decreases at higher FRs (Figure S7I), they are very variable (Mathy et al., 2009) when voltage states, CF activation phase, or CF input conductance are varied. Sometimes, there is even no “obvious” pause following a CS.

The CF input itself is not “all-or-none” either. The variable number of spikes per CF burst can affect both somatic and dendritic responses (Mathy et al., 2009) (Figure S1). Furthermore, CF synaptic inputs can undergo PPD (Andjus et al., 2005), LTD (Hansel and Linden, 2000), and regulation by norepinephrine (Carey and Regehr, 2009). All of them can depress the CF EPSC to modulate somatic and dendritic responses (Figure 7). In particular, PPD bridges the gap between instantaneous CF FRs and varied CS spikelet numbers (Burroughs et al., 2017; Khaliq and Raman, 2005; Maruta et al., 2007; Warnaar et al., 2015) and can play an important role in regulating CF responses.

EXPERIMENTAL PROCEDURES

All simulations were performed with NEURON, version 7.4 (Hines and Carnevale, 1997). We use the morphology of a 21-day-old Wistar rat PC (Roth and Häusser, 2001). As shown in Figure 2A, the model consists of an AIS (purple), a soma (red), smooth dendrites (black), and spiny dendrites (gray). The first 17 μm of the reconstructed axon are preserved as the AIS. When exploring the spike initiation site, AIS indicates the end next to the myelinated axon. The model has following passive parameters: $R_m = 120.2 \text{ k}\Omega \text{ cm}^2$, $R_i = 120 \text{ }\Omega \text{ cm}$, and $C_m = 0.64 \text{ }\mu\text{F/cm}^2$. To compensate for the absence of spines in the reconstructed morphology, the conductance of passive current and C_m are scaled by a factor of 5.3 in the spiny dendrite and 1.2 in the smooth dendrite. The conductance densities of ionic currents in different parts of the model were found by hand tuning. Detailed information about ionic current equations and the process of parameter tuning can be found in Supplemental Experimental Procedures.

The spiking threshold of SSs was defined as the membrane potential at which $dv/dt = 20 \text{ mV/ms}$. The synaptic conductance activated by CF input is approximated as a bi-exponential waveform, with 0.3 and 3 ms as the rise and decay time constants (Davie et al., 2008). The peak conductance of baseline CF input is 1.2 nS. 500 synaptic inputs are distributed on the soma and smooth dendrite at a constant density per length to simulate the CF input. The conductance varies in the range of 80%–100% to simulate the EPSC changes by PPD. Due to the elaborate structure, the dendrite is not isopotential with the soma when holding current is injected at the soma. The somatic membrane potential is used to represent the voltage state of the PC except in Figure 4, in which dendritic membrane potential is used. When measuring the distance dependence of the peak dendritic response, we selected the first dendritic spikelet if there were two spikelets. To measure the excitability of individual branches, we define a measure as the ratio of the spiny dendrite capacitance load to CF synaptic input, load/input ratio, which can be transformed into “area of spiny dendrite”/“length of smooth dendrite” within each branch in the model. To exclude the effect of phase dependence on CSs in Figure 5, all the CF signals are activated with 3 ms after the preceding SS under different voltage states. To explore how simultaneous clustered synaptic inputs regulate dendritic response and somatic output, PF or stellate cell synaptic inputs are activated 5 ms after the CF input (Figure 6). To simply mimic the PC voltage states *in vivo*,

1,105 PF synapses and 1,105 inhibitory synapses are uniformly distributed on the spiny dendrites. Different voltage states of the PC are achieved by randomly activating excitatory and inhibitory synapses at different average FRs. To estimate the energy cost of spikes, we computed the Na^+ (three Na^+ ions consume one ATP molecule) and Ca^{2+} influx (one Ca^{2+} ion consumes one ATP molecule) during a spike in the whole PC (AIS, soma, and dendrite) (Attwell and Laughlin, 2001).

DATA AND SOFTWARE AVAILABILITY

The accession number for the model code reported in this study is ModelDB: 243446.

SUPPLEMENTAL INFORMATION

Supplemental Information includes Supplemental Experimental Procedures and nine figures and can be found with this article online at <https://doi.org/10.1016/j.celrep.2018.07.011>.

ACKNOWLEDGMENTS

We thank Ede Rancz, Michael Häusser, Gen Ohtsuki, Christian Hansel, João Couto (the data shared by the above-mentioned people were used in the manuscript for validation of the simulation results), Bruce Bean, Indira Raman (the data shared by the above-mentioned people were used to constrain ionic current properties), Matthew Nolan, Edward Zagher, Bernardo Rudy, and Paul Mathews for sharing related experimental data for us to understand PC properties. This work was supported by the Okinawa Institute of Science and Technology Graduate University.

AUTHOR CONTRIBUTIONS

Y.Z., S.D., and E.D.S. conceived this study. Y.Z. performed all the simulations. Y.Z. and E.D.S. analyzed the simulation data. Y.Z. and E.D.S. wrote and revised the manuscript.

DECLARATION OF INTERESTS

The authors declare no competing interests.

Received: November 29, 2017

Revised: May 27, 2018

Accepted: July 1, 2018

Published: August 7, 2018

REFERENCES

- Albus, J.S. (1971). A theory of cerebellar function. *Math. Biosci.* 10, 25–61.
- Andjus, P.R., Bajic, A., Zhu, L., Schachner, M., and Strata, P. (2005). Short-term facilitation and depression in the cerebellum: some observations on wild-type and mutant rodents deficient in the extracellular matrix molecule tenascin C. *Ann. N Y Acad. Sci.* 1048, 185–197.
- Anwar, H., Hepburn, I., Nedelcescu, H., Chen, W., and De Schutter, E. (2013). Stochastic calcium mechanisms cause dendritic calcium spike variability. *J. Neurosci.* 33, 15848–15867.
- Attwell, D., and Laughlin, S.B. (2001). An energy budget for signaling in the grey matter of the brain. *J. Cereb. Blood Flow Metab.* 21, 1133–1145.
- Bekkers, J.M., and Häusser, M. (2007). Targeted dendrotomy reveals active and passive contributions of the dendritic tree to synaptic integration and neuronal output. *Proc. Natl. Acad. Sci. USA* 104, 11447–11452.
- Burroughs, A., Wise, A.K., Xiao, J., Houghton, C., Tang, T., Suh, C.Y., Lang, E.J., Apps, R., and Cerminara, N.L. (2017). The dynamic relationship between cerebellar Purkinje cell simple spikes and the spikelet number of complex spikes. *J. Physiol.* 595, 283–299.

- Carey, M.R., and Regehr, W.G. (2009). Noradrenergic control of associative synaptic plasticity by selective modulation of instructive signals. *Neuron* 62, 112–122.
- Carter, B.C., and Bean, B.P. (2009). Sodium entry during action potentials of mammalian neurons: incomplete inactivation and reduced metabolic efficiency in fast-spiking neurons. *Neuron* 64, 898–909.
- Carter, B.C., and Bean, B.P. (2011). Incomplete inactivation and rapid recovery of voltage-dependent sodium channels during high-frequency firing in cerebellar Purkinje neurons. *J. Neurophysiol.* 105, 860–871.
- Cerminara, N.L., and Rawson, J.A. (2004). Evidence that climbing fibers control an intrinsic spike generator in cerebellar Purkinje cells. *J. Neurosci.* 24, 4510–4517.
- Coesmans, M., Weber, J.T., De Zeeuw, C.I., and Hansel, C. (2004). Bidirectional parallel fiber plasticity in the cerebellum under climbing fiber control. *Neuron* 44, 691–700.
- Davie, J.T., Clark, B.A., and Häusser, M. (2008). The origin of the complex spike in cerebellar Purkinje cells. *J. Neurosci.* 28, 7599–7609.
- De Schutter, E., and Bower, J.M. (1994a). An active membrane model of the cerebellar Purkinje cell. II. Simulation of synaptic responses. *J. Neurophysiol.* 71, 401–419.
- De Schutter, E., and Bower, J.M. (1994b). An active membrane model of the cerebellar Purkinje cell. I. Simulation of current clamps in slice. *J. Neurophysiol.* 71, 375–400.
- Deneux, T., Kaszas, A., Szalay, G., Katona, G., Lakner, T., Grinvald, A., Rózsa, B., and Vanzetta, I. (2016). Accurate spike estimation from noisy calcium signals for ultrafast three-dimensional imaging of large neuronal populations in vivo. *Nat. Commun.* 7, 12190.
- Fernandez, F.R., Engbers, J.D., and Turner, R.W. (2007). Firing dynamics of cerebellar Purkinje cells. *J. Neurophysiol.* 98, 278–294.
- Gallimore, A.R., Kim, T., Tanaka-Yamamoto, K., and De Schutter, E. (2018). Switching on depression and potentiation in the cerebellum. *Cell Rep.* 22, 722–733.
- Gilbert, P.F. (1976). Simple spike frequency and the number of secondary spikes in the complex spike of the cerebellar Purkinje cell. *Brain Res.* 114, 334–338.
- Hansel, C., and Linden, D.J. (2000). Long-term depression of the cerebellar climbing fiber–Purkinje neuron synapse. *Neuron* 26, 473–482.
- Hines, M.L., and Carnevale, N.T. (1997). The NEURON simulation environment. *Neural Comput.* 9, 1179–1209.
- Ito, M. (1972). Neural design of the cerebellar motor control system. *Brain Res.* 40, 81–84.
- Jelitai, M., Puggioni, P., Ishikawa, T., Rinaldi, A., and Duguid, I. (2016). Dendritic excitation-inhibition balance shapes cerebellar output during motor behaviour. *Nat. Commun.* 7, 13722.
- Khalik, Z.M., and Raman, I.M. (2005). Axonal propagation of simple and complex spikes in cerebellar Purkinje neurons. *J. Neurosci.* 25, 454–463.
- Khalik, Z.M., Gouwens, N.W., and Raman, I.M. (2003). The contribution of resurgent sodium current to high-frequency firing in Purkinje neurons: an experimental and modeling study. *J. Neurosci.* 23, 4899–4912.
- Khavandgar, S., Walter, J.T., Sageser, K., and Khodakhah, K. (2005). Kv1 channels selectively prevent dendritic hyperexcitability in rat Purkinje cells. *J. Physiol.* 569, 545–557.
- Kitamura, K., and Häusser, M. (2011). Dendritic calcium signaling triggered by spontaneous and sensory-evoked climbing fiber input to cerebellar Purkinje cells in vivo. *J. Neurosci.* 31, 10847–10858.
- Linás, R., and Sugimori, M. (1980). Electrophysiological properties of in vitro Purkinje cell dendrites in mammalian cerebellar slices. *J. Physiol.* 305, 197–213.
- Mano, N. (1970). Changes of simple and complex spike activity of cerebellar Purkinje cells with sleep and waking. *Science* 170, 1325–1327.
- Marr, D. (1969). A theory of cerebellar cortex. *J. Physiol.* 202, 437–470.
- Martina, M., Yao, G.L., and Bean, B.P. (2003). Properties and functional role of voltage-dependent potassium channels in dendrites of rat cerebellar Purkinje neurons. *J. Neurosci.* 23, 5698–5707.
- Martina, M., Metz, A.E., and Bean, B.P. (2007). Voltage-dependent potassium currents during fast spikes of rat cerebellar Purkinje neurons: inhibition by BDS-I toxin. *J. Neurophysiol.* 97, 563–571.
- Maruta, J., Hensbroek, R.A., and Simpson, J.I. (2007). Intraburst and interburst signaling by climbing fibers. *J. Neurosci.* 27, 11263–11270.
- Masoli, S., Solinas, S., and D’Angelo, E. (2015). Action potential processing in a detailed Purkinje cell model reveals a critical role for axonal compartmentalization. *Front. Cell. Neurosci.* 9, 47.
- Mathy, A., Ho, S.S., Davie, J.T., Duguid, I.C., Clark, B.A., and Häusser, M. (2009). Encoding of oscillations by axonal bursts in inferior olive neurons. *Neuron* 62, 388–399.
- Monsivais, P., Clark, B.A., Roth, A., and Häusser, M. (2005). Determinants of action potential propagation in cerebellar Purkinje cell axons. *J. Neurosci.* 25, 464–472.
- Najafi, F., Giovannucci, A., Wang, S.S., and Medina, J.F. (2014). Coding of stimulus strength via analog calcium signals in Purkinje cell dendrites of awake mice. *eLife* 3, e03663.
- Ohtsuki, G., Piochon, C., Adelman, J.P., and Hansel, C. (2012). SK2 channel modulation contributes to compartment-specific dendritic plasticity in cerebellar Purkinje cells. *Neuron* 75, 108–120.
- Otsu, Y., Marcaggi, P., Feltz, A., Isope, P., Kollo, M., Nusser, Z., Mathieu, B., Kano, M., Tsujita, M., Sakimura, K., and Dieudonné, S. (2014). Activity-dependent gating of calcium spikes by A-type K⁺ channels controls climbing fiber signaling in Purkinje cell dendrites. *Neuron* 84, 137–151.
- Palmer, L.M., Clark, B.A., Gründemann, J., Roth, A., Stuart, G.J., and Häusser, M. (2010). Initiation of simple and complex spikes in cerebellar Purkinje cells. *J. Physiol.* 588, 1709–1717.
- Piochon, C., Tittley, H.K., Simmons, D.H., Grasselli, G., Elgersma, Y., and Hansel, C. (2016). Calcium threshold shift enables frequency-independent control of plasticity by an instructive signal. *Proc. Natl. Acad. Sci. USA* 113, 13221–13226.
- Rancz, E.A., and Häusser, M. (2010). Dendritic spikes mediate negative synaptic gain control in cerebellar Purkinje cells. *Proc. Natl. Acad. Sci. USA* 107, 22284–22289.
- Rokni, D., Tal, Z., Byk, H., and Yarom, Y. (2009). Regularity, variability and bistability in the activity of cerebellar Purkinje cells. *Front. Cell. Neurosci.* 3, 12.
- Roth, A., and Häusser, M. (2001). Compartmental models of rat cerebellar Purkinje cells based on simultaneous somatic and dendritic patch-clamp recordings. *J. Physiol.* 535, 445–472.
- Schmolesky, M.T., Weber, J.T., De Zeeuw, C.I., and Hansel, C. (2002). The making of a complex spike: ionic composition and plasticity. *Ann. N Y Acad. Sci.* 978, 359–390.
- Steuber, V., Mittmann, W., Hoebeek, F.E., Silver, R.A., De Zeeuw, C.I., Häusser, M., and De Schutter, E. (2007). Cerebellar LTD and pattern recognition by Purkinje cells. *Neuron* 54, 121–136.
- Stuart, G., and Häusser, M. (1994). Initiation and spread of sodium action potentials in cerebellar Purkinje cells. *Neuron* 13, 703–712.
- Swensen, A.M., and Bean, B.P. (2003). Ionic mechanisms of burst firing in dissociated Purkinje neurons. *J. Neurosci.* 23, 9650–9663.
- Vetter, P., Roth, A., and Häusser, M. (2001). Propagation of action potentials in dendrites depends on dendritic morphology. *J. Neurophysiol.* 85, 926–937.
- Wang, S.S., Denk, W., and Häusser, M. (2000). Coincidence detection in single dendritic spines mediated by calcium release. *Nat. Neurosci.* 3, 1266–1273.
- Warnaar, P., Couto, J., Negrello, M., Junker, M., Smilgin, A., Ignashchenkova, A., Giugliano, M., Thier, P., and De Schutter, E. (2015). Duration of Purkinje cell complex spikes increases with their firing frequency. *Front. Cell. Neurosci.* 9, 122.

Wilms, C.D., and Häusser, M. (2015). Reading out a spatiotemporal population code by imaging neighbouring parallel fibre axons in vivo. *Nat. Commun.* 6, 6464.

Womack, M.D., and Khodakhah, K. (2003). Somatic and dendritic small-conductance calcium-activated potassium channels regulate the output of cerebellar Purkinje neurons. *J. Neurosci.* 23, 2600–2607.

Yang, Y., and Lisberger, S.G. (2014). Purkinje-cell plasticity and cerebellar motor learning are graded by complex-spike duration. *Nature* 510, 529–532.

Zagha, E., Manita, S., Ross, W.N., and Rudy, B. (2010). Dendritic Kv3.3 potassium channels in cerebellar purkinje cells regulate generation and spatial dynamics of dendritic Ca²⁺ spikes. *J. Neurophysiol.* 103, 3516–3525.